*Progress In Electromagnetics Research C, Vol. 103, 187–197, 2020*

# Design of an Ultra Wide Band Antenna Based on a SIW Resonator

**Massimo Donelli[1, *], Sreedevi K. Menon[2], Giada Marchi[1, 3], Viviana Mulloni[3], and Mohammedhusen Manekiya[1]**

**Abstract**—In this work, the design of an ultra-wideband (UWB) fork monopole antenna based on a substrate integrated waveguide (SIW) resonator has been proposed. The SIW resonator not only improves the antenna bandwidth and its performances, but also permits to reduce the antenna size and weight. An antenna prototype has been designed, fabricated, and experimentally assessed. The obtained results are quite satisfactory, and they demonstrate the potentialities of the proposed geometry.

## 1. INTRODUCTION

In the past decades, wireless systems and handy devices such as mobile phones and tablets were able to provide different services and tools which require high bandwidth and channel capabilities [1, 2]. The recent development of digital transformation and industry 4.0 lead to a dramatic evolution and diffusion of wireless sensors. One of the critical points of any wireless devices is the antenna since it must be compact, broadband, and characterized by a high gain. Ultra-wideband (UWB) techniques permit to manage the frequency spectra efficiently and to obtain high spatial resolutions; moreover, UWB antenna structures are well known in scientific literature and simple to fabricate [3–7]. They have been successfully adopted in different practical applications such as radar systems able to provide fine spatial resolution for range measurements, through the wall applications for homeland security [8], microwave imaging systems, non-invasive monitoring of heartbeat and breath, and other interesting biomedical applications [9]. However, as stated above, the modern wireless system requires a continuous progress in terms of miniaturization, efficiency, and band occupation [10–12]. UWB multiple input multiple output (MIMO) antennas permit to obtain high efficiency and optimal use of the wireless channel. However, they usually require different antenna elements and strong miniaturization which cannot be easily achieved [13, 14]. Attempts to obtain compact antenna structures have been made by considering fractal geometries. Even though the good results in terms of miniaturization are obtained for fractal antenna geometries, they are problematic from the point of view of the fabrication due to mechanical constraints [15]. Recently, the use of substrate integrated waveguide resonators [16–22] could solve the problem of antenna miniaturization in an easy way. Substrate integrated waveguide (SIW) can be easily integrated into a planar structure like microstrip line, rectangular antenna patch as well as into a nonplanar structure like waveguide thus combining the advantages of both structures [23, 24]. Thanks to SIW technique, classical waveguide structures or resonators (characterized by a very high-quality factor) can now be fabricated in microstrip technology by simply using metallized vias or holes in dielectric substrates. SIW not only has the advantages of classical microstrip circuit such as low cost, easiness of fabrication, and compact size but also provides high performances, in terms of the quality factor, which up to now can be only offered by waveguides, which are bulky and expensive metallic structures. One of the first integrations of a passive SIW component was proposed for the design of a

*Received 4 February 2020, Accepted 5 June 2020, Scheduled 8 July 2020*

* Corresponding author: Massimo Donelli (massimo.donelli@unitn.it).

[1] Department of Information Engineering and Computer Science, University of Trento, 38100, Italy. [2] Department of Electronics and Communication Engineering, Amrita Vishwa Vidyapeetham, India. [3] Center for Materials and Microsystems (CMM), Fondazione Bruno Kessler (FBK), Italy

microwave filter based on inductive-post, which allows higher quality factor with respect to microstrip technology [25]. Chipless radio-frequency identification (RFID) tags based on a set of SIW resonators have been proposed. The obtained experimental results demonstrated the positive effects of the SIW cavity use. The obtained antenna prototype is compact, cheap, and shows very good performances in the whole considered frequency range. The paper is organized as follows. Section 2 presents a detailed description of the proposed antenna design and its optimization procedure based on a customized version of a particle swarm optimizer PSO. In Section 3, an experimental antenna prototype, obtained with the design methodology previously described is numerically and experimentally assessed. Finally, Section 4 reports the conclusions.

## 2. DESIGN OF THE ANTENNA STRUCTURE

The UWB antenna structure is reported in Fig. 1. A fork monopole antenna with a microstrip feeding line of width $w_0$ is proposed, according to [26]. The ground plane is printed on the back side of the dielectric substrate, and it consists of a strip of copper of height and width $h_0$ and $w_0 + S_2 + S_3$ with reference to Fig. 1, respectively. The fork monopole is backed with a surface integrated waveguide SIW cavity obtained with a set of metallized vias. The SIW cavity is aimed at improving the antenna performances in terms of return loss of $S_{11}$. With reference to Fig. 1 the SIW cavity consists of sixteen metallized holes of diameter $D$; the inter-element hole space is $S_0$; and the distance of the two holes rows from the fork monopole arms is $S_1$. The resonance frequency of the SIW cavity is provided by the following relation [22–25]:

$$f_{TE_{m0q}} = \frac{C_0}{2\sqrt{\varepsilon_r}} \sqrt{\left(\frac{m}{W_{eff}}\right)^2 + \left(\frac{q}{L_{eff}}\right)^2} \tag{1}$$

where $\varepsilon_r$ is the dielectric permittivity of the considered dielectric substrate; $C_0$ is the light velocity; $m$ and $q$ represent the two indexes of the transverse electric propagation mode.

$$L_{eff} = ((N-1)\, S_0 + D) - \frac{D^2}{0.95 S_0} \tag{2}$$

$$W_{eff} = 2\left(S_1 + w_1 + \frac{w_2}{2}\right) - \frac{D^2}{0.95 S_0} \tag{3}$$

where $S_0$ is the distance between via centres, $D$ the via diameter, $N$ the via number, and the term $((N-1)\, S_0 + D)$ represents the length of the SIW cavity. In the considered structure, the SIW resonator is directly excited by the structure of UWB antenna; therefore, empirical tuning of parameters $D$, $S_0$, and

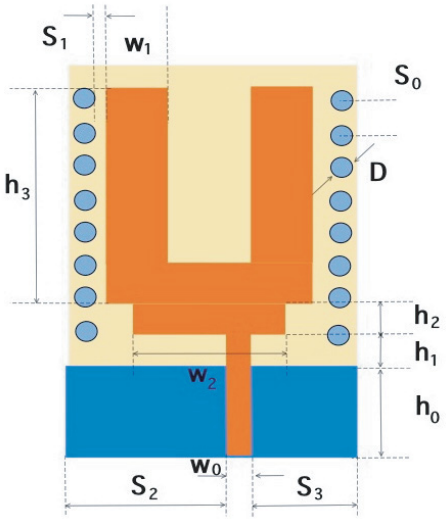


**Figure 1.** Antenna geometry.

$w_1$ is mandatory. In order to obtain a high performance antenna, all the geometrical parameters reported in Fig. 1 must be accurately tuned. In order to accomplish this task, an unsupervised methodology based on an evolutionary algorithm, namely the particle swarm optimizer (PSO) has been considered. The antenna design, based on microstrip technology, has been formulated as an optimization problem [27–29]. The process goals are fixed with reference to the impedance matching at the antenna input port ($S_{11}$ values). In particular, an $|S_{11}| \leq -10[dB]$ in the frequency range $3\,GHz \leq f_w \leq 11\,\text{GHz}$ has been considered as objective for the optimization procedure, where $f_w$ is the working frequency. The antenna structure is uniquely identified by considering the following geometrical parameters (with reference to Fig. 1) $\underline{X} = \{w_0, w_1, w_2, S_0, S_1, S_2, S_3, h_0, h_1, h_2, D\}$. In order to meet the requirements, a suitable cost function reported in the following relation has been defined:

$$\Gamma\left(\underline{X}\right) = \Sigma_{m=1}^{M} \max\left\{0; \frac{\vartheta\left(m\Delta f, \underline{X}\right) - |S_{11}|_{req}}{|S_{11}|_{req}}\right\} \tag{4}$$

where $\Delta f$ is the considered frequency step in the operative range $3\,GHz \leq f_w \leq 11\,\text{GHz}$, and $|S_{11}|_{req}$ represents the return loss constraints expressed in dB. The term $\vartheta\left(m\Delta f, \underline{X}\right)$ represents the return loss value obtained at frequency $m\Delta f$ when a trial antenna geometry defined by the vector $\underline{X}$ is considered. It is worth noticing that relation in Eq. (4) represents the difference between the return loss requirements and the performances of a trial antenna geometry. In order to obtain an optimized antenna relation Eq. (4) is minimized with a customized version of PSO. To estimate the characteristics of trial antennas, provided by the term $(m\Delta f, \underline{X})$, a suitable geometrical generator combined with a commercial electromagnetic simulator (namely ADS by Keysight) is considered. The minimization of the relation in Eq. (4) is obtained with a set of trial solutions $\underline{X}_j^k$ where $k = 1, \ldots, K_{\max}$ is the iteration number, and $J$ is the trial solution index. The set of trial solutions is constructed following the PSO rules. The optimizer continues to tune the geometrical parameters $\underline{X}_j^k$ until the stopping criteria related to the maximum iteration number $k = K_{\max}$ or a threshold on the cost function $\Gamma\left(\underline{X}_m^k\right) \leq \eta$ is reached. When the optimizer reaches a satisfactory solution, the optimal geometrical parameters defined as $\underline{X}^{opt} = \arg\left\{\min\left[\Gamma\left(\underline{X}_k\right)\right]\right\}$ are stored and used to fabricate the antenna. In particular, the optimization procedure based on the PSO optimizer has been initialized with a population of $M = 5$ particles (which are aimed at encoding the trial antenna geometrical parameters) randomly initialized and used as a starting point for the optimizer. Concerning the other specific PSO parameters a threshold on the fitness of $\eta = 10^{-3}$, a maximum number of iterations $K_{\max} = 100$, and a constant inertial weight $I_{weight} = 0.4$ were used. The remaining PSO parameters have been chosen according to the guidelines reported in the reference literature [30]. It is worth noticing that the optimization procedure has been initialized with completely random values as in [30]. The antenna geometry has been optimized by using a serial machine equipped with 16 Gigabyte of memory and four processors. Each iteration of the optimization procedure required about 40 seconds and the whole design about one hour. To simulate the antenna structure, a commercial electromagnetic simulator, namely ADS from keysight company, which permits to simulate complex structures with a high degree of accuracy and a very limited computational time. The optimized geometrical parameters obtained after the design procedure are reported in Table 1. $H_t$ and $W_t$ reported in Table 1 represent the total height and width, respectively. An experimental prototype has been fabricated considering the geometrical parameters reported in Table 1 and a ceramic dielectric substrate namely ARLON 25N, $\varepsilon_r = 3.38$, $tan\left(\delta\right) = 10^{-3}$, and thickness $t = 0.8\,\text{mm}$. The main body of the antenna, consisting of a fork dipole, has been obtained by using a CNC miling machine with an accuracy $\delta = 0.02\,\text{mm}$. The realization process of the SIW cavity is summarized in Fig. 2, and it requires the creation of metallized vias, covering the internal surface of the holes with copper. In particular, to implement the metallization process, the antenna prototype was covered with a dry film

**Table 1.** Geometrical antenna parameters obatined after the optimization procedure. A ceramic dielectric substrate of ARLON 25N, $\varepsilon_r = 3.38$, $\tan\left(\delta\right) = 10^{-3}$, and thickness $t = 0.8\,\text{mm}$ has been considered.

| Parameter | $w_0$ | $w_1$ | $w_2$ | $S_0$ | $S_1$ | $S_2$ | $S_3$ | $h_0$ | $h_1$ | $h_2$ | $D$ | $h_3$ | $H_t$ | $W_t$ |
|---|---|---|---|---|---|---|---|---|---|---|---|---|---|---|
| [mm] | 1.91 | 5.00 | 9.91 | 2.50 | 1.01 | 16.80 | 10.09 | 7.55 | 0.45 | 2.00 | 1.5 | 16.80 | 27.00 | 28.80 |

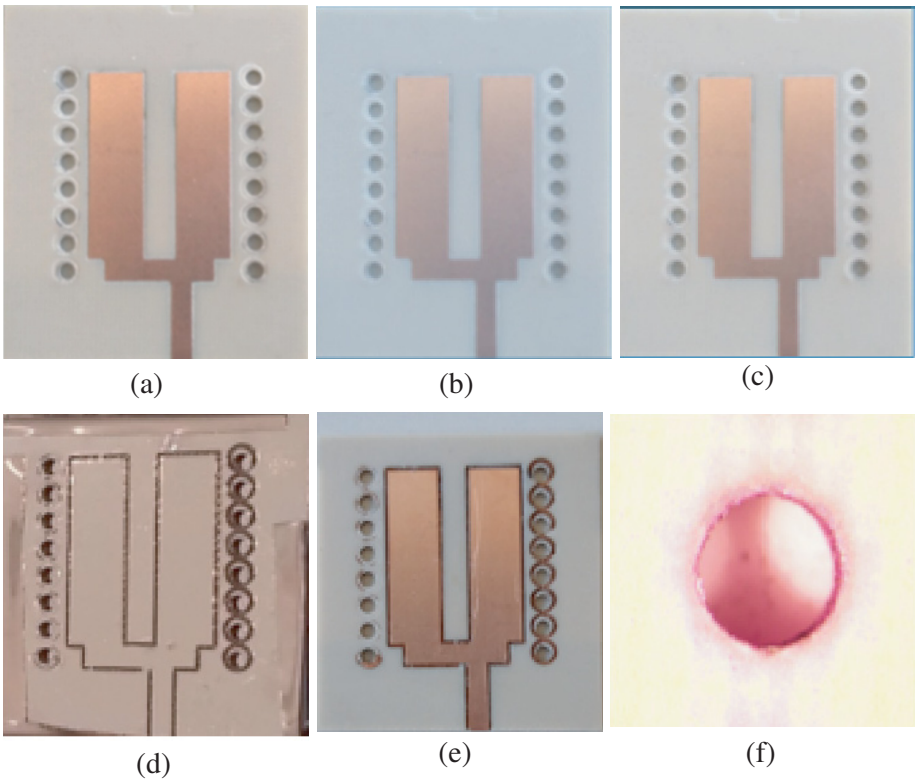


**Figure 2.** Copper vias metalization procedure, (a) original antenna fabricated by CNC milling, (b) dry film lamination, (c) process of removal of protective sheet, which removes also the dry film above the holes, (d) after copper evaporation, (e) dry film removal, (f) hole metallization seen from antenna bottomside.

layer on the front side and then heated at $120°C$ for 1 minute to improve the dry film adhesion. After cooling, the dry film protective cover was removed, also removing the dry film above the holes. The antenna prototype was then inserted in an evaporation chamber supported by a 6-inch silicon wafer and firmly attached to it with adhesive Kapton tape. A copper film of a nominal thickness of $1.5\mu m$ was deposited by e-gun evaporation under vacuum at room temperature. The antennas were then detached from the support and immersed in a KOH concentrated (10%) solution in order to remove the dry film and the copper above it by lift-off. Photos of the top and bottom sides of the antenna prototype, equipped with a sub-miniature type A (SMA) coaxial connectors, are shown in Fig. 3.

## 3. EXPERIMENTAL ASSESSMENT

In order to assess the antenna capabilities in terms of return loss and beam pattern, an experimental setup has been arranged inside an anechoic chamber. The antenna $|S_{11}|$ has been measured by means of a Vector Network Analyser (VNA). Fig. 4 reports the experimental data with those obtained by simulation using ADS software. An antenna prototype without the SIW structure has also been measured to evaluate the effect of the SIW cavity. As can be noticed, $|S_{11}|$ of the prototype equipped with the SIW cavity (green dotted line) meets the initial requirements: in particular the return loss for the whole considered frequency band is found to be well below the initial requirements of about $-10\,\text{dB}$. The dotted black line represents the reference level. For the sake of comparisons, the measurements have been compared with numerical data obtained with the ADS commercial software. As can be noticed from the data reported in Fig. 4, the agreement between numerical and experimental data is quite satisfactory. There is only a strange spike in the numerical data located near a frequency of $f = 2.8\,\text{GHz}$, and the spike is not present in the experimental measurements. It is worth noticing that

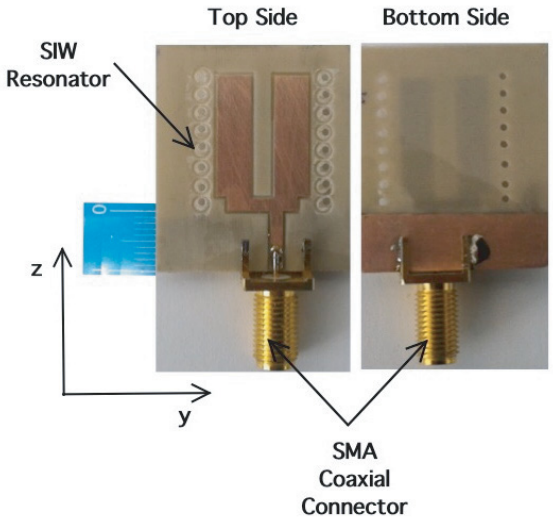


**Figure 3.** Photos of the UWB antenna prototype.

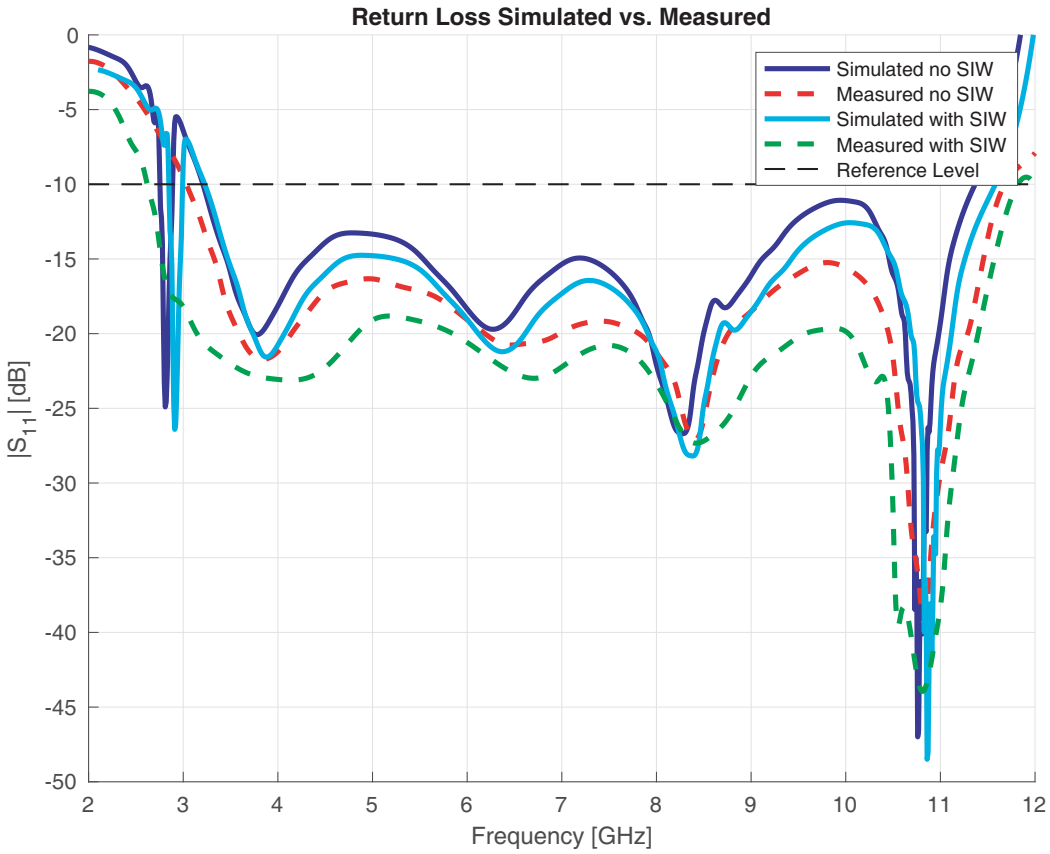


**Figure 4.** Numerical versus measured antenna return loss $S_{11}$.

the simulation has been performed without considering the SMA coaxial connector, and a hypothesis of the absence of the spike at $f = 2.8$ GHz in the measurements could be the presence of the SMA coaxial connector. The measurement obtained without the SIW cavity (red dotted line) shows lower performances than the prototype equipped with the SIW cavity. In particular, in the frequency range between 9 and 10 GHz the return loss is higher, and it reaches a value up to 5 dB, for the prototype with

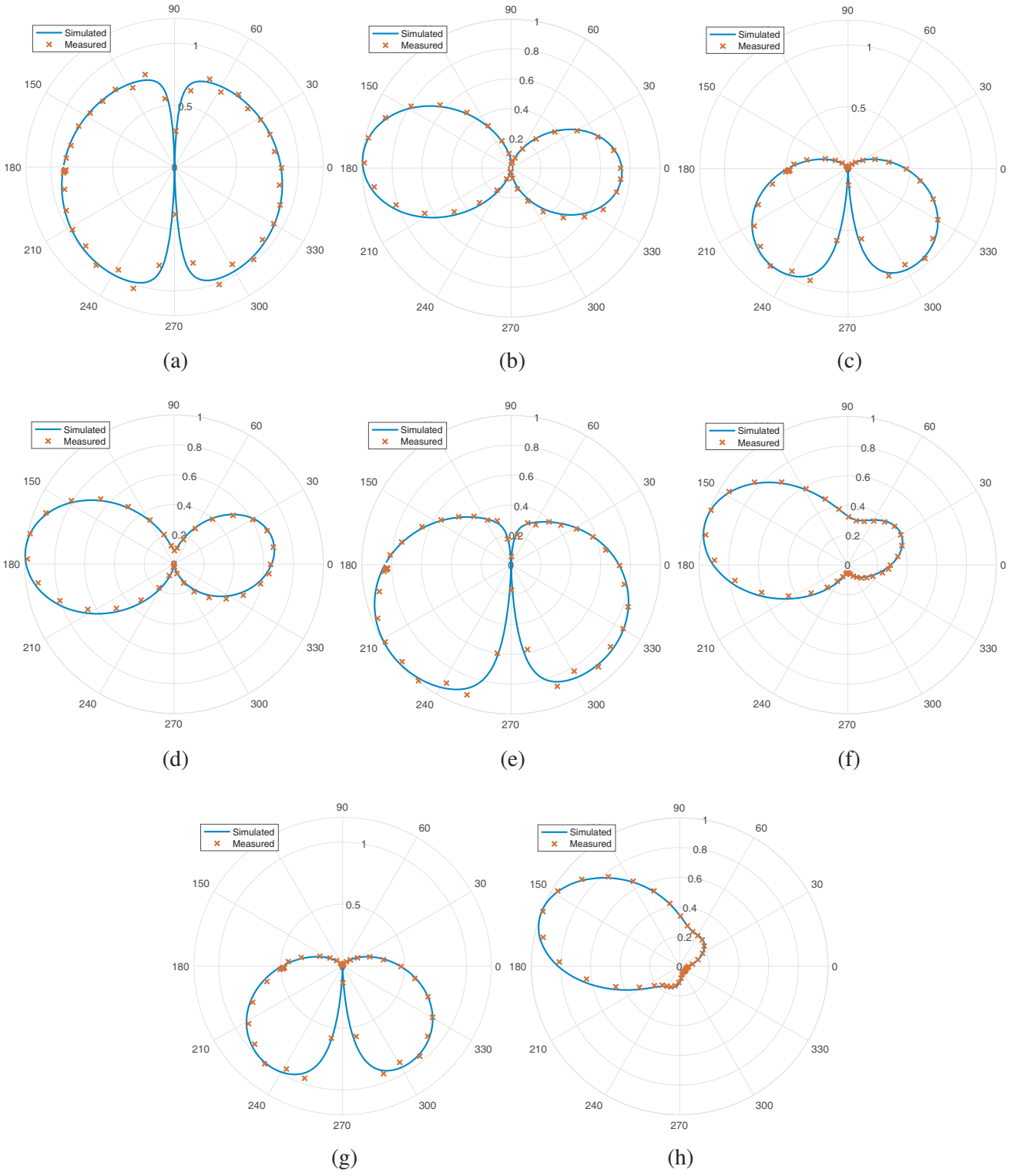


**Figure 5.** Simulated vs. measured antenna beam patterns, (a) $E$-plane (b) $H$-plane 3 GHz, (c) $E$-plane (d) $H$-plane 4 GHz, (e) $E$-plane (f) $H$-plane 5 GHz,(g) $E$-plane (h) $H$-plane 6 GHz. The $E$ and $H$ planes correspond to the $xz$ and $xy$ planes respectively.

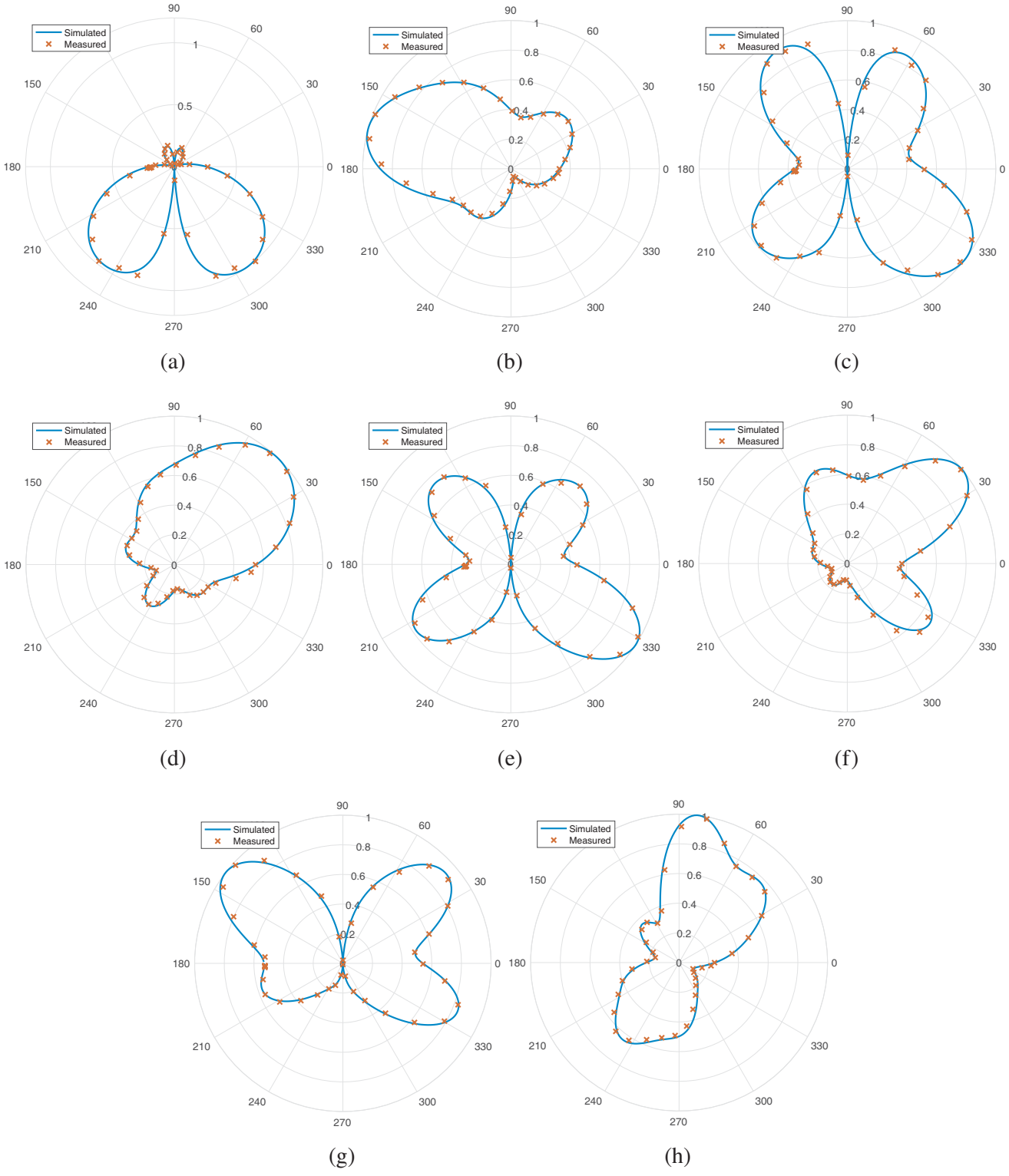


**Figure 6.** Simulated vs. measured antenna beam patterns, (a) $E$-plane (b) $H$-plane 7 GHz, (c) $E$-plane (d) $H$-plane 8 GHz, (e) $E$-plane (f) $H$-plane 9 GHz,(g) $E$-plane (h) $H$-plane 10 GHz. The $E$ and $H$ planes correspond to the $xz$ and $xy$ planes respectively.

the SIW cavity. The antenna beam pattern has been measured in both the $E$ and $H$-planes for 3 GHz, 4 GHz, 5 GHz, 6 GHz, 7 GHz, 8 GHz, 9 GHz, and 10 GHz. The antenna prototype has been placed on a mechanical pedestal, and the beam pattern has been estimated by considering an angular step of ten degrees. The measurements have been compared with the numerical results obtained with ADS, and the data are reported in Figs. 5 and 6. As can be noticed from the data of Figs. 5 and 6, which report the normalized electric fields in the horizontal and vertical planes, the agreement between simulated and experimental data is very good. The obtained beam patterns are not omnidirectional; therefore, this antenna is not particularly suitable for mobile phone applications, but it can be efficiently adopted, to provide links between sensor nodes in wireless sensor network applications. It is worth noticing that the main requirement of the Federal Communication Commission (FCC) for an UWB antenna is that it must have an operative bandwidth of at least 500 MHz. $S_{f11}$ versus frequency reported in Fig. 7 shows that the antenna bandwidth is about 8.5 GHz; therefore, it perfectly accomplishes the Federal Communication Commission requirements for UWB.

The values of antenna gain versus frequency are reported in Fig. 7. The antenna gain has been estimated in the anechoic chamber with the three antenna method. In particular the gains, with and without the SIW structure, are numerically and experimentally measured and compared in Fig. 7. As can be noticed the introduction of the SIW structure improves the gain about 3 dBi demonstrating the effectiveness of the two via rows. The numerical estimation of the radiation efficiency versus frequency is reported in Fig. 8. The data reported in Fig. 8 demonstrate the efficiency of the antenna always between 80% and 100% in the frequency band of interest, and the introduction of the SIW structure produces only a slight improvement of the antenna radiation efficiency especially at higher frequency. For the sake of completeness, the current distributions as in [31–34] for six different working frequencies are reported in Figs. 9(a)–(f). It is quite evident how the current is able to correctly flow through the microstrip feeding line, demonstrating the good matching, then the current flow along the fork arms

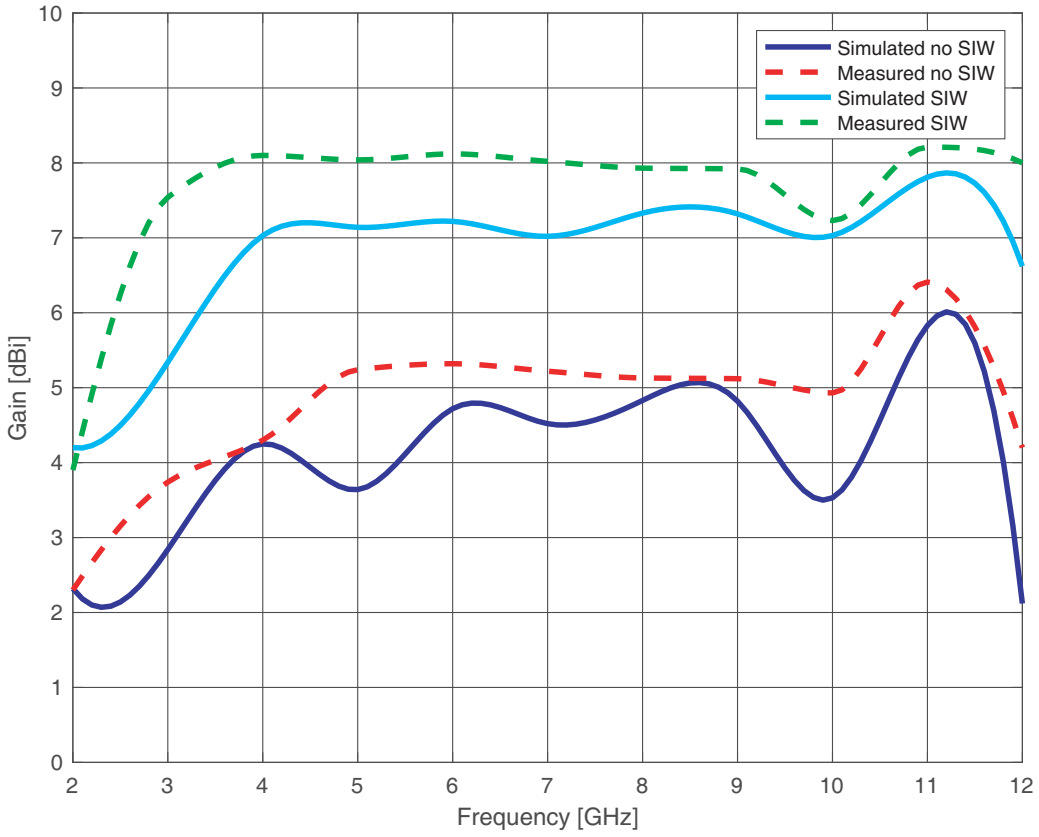


**Figure 7.** Antenna gain vs. frequency, simulated and measured values estimated with and without the SIW structure.

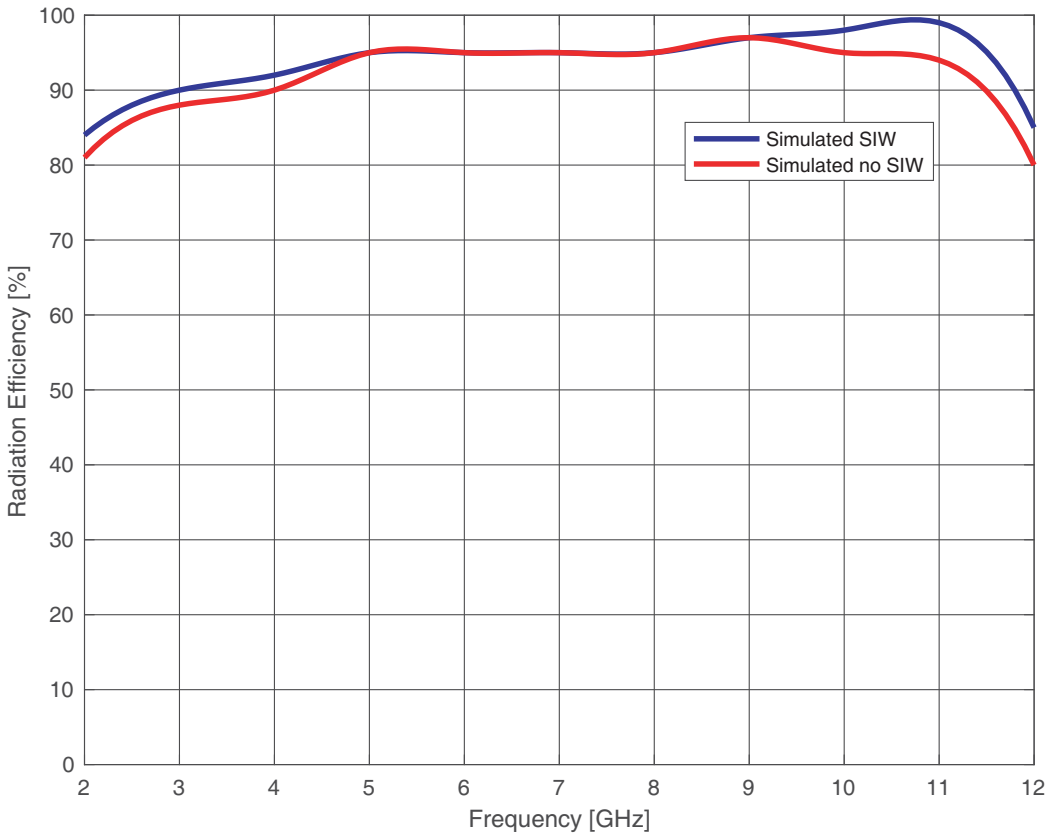


**Figure 8.** Radiation Efficiency vs. frequency estimated with and without the SIW structure.

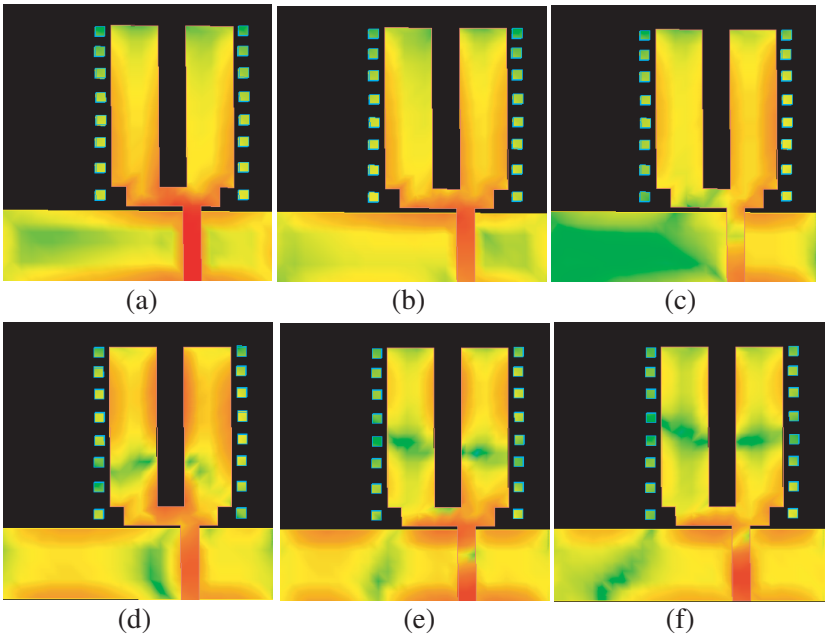


**Figure 9.** Current distribution on the antenna surface, (a) 2.0 GHz (b) 4.0 GHz, (c) 6.0 GHz, (d) 8.0 GHz, (e) 10.0 GHz, (f) 12.0 GHz.

permits a good propagation of the electromagnetic waves in the wireless channel. Figs. 9 are freeze snapshots of the surface current propagation animation produced by means of the ADS software. No current reflected back is observed during the simulation demonstrating the good antenna matching.

## 4. CONCLUSION

In this work, the design of a UWB antenna based on a SIW resonator has been designed, fabricated, numerically and experimentally assessed. The obtained antenna prototype provides good radiation, return loss characteristics, and a bandwidth in the range from 3 GHz to 11 GHz. The agreement between measured and simulated data is very good. The antenna size is very small, confirming that it is a good candidate for modern handheld UWB systems.

## REFERENCES

1. Challita, F., et al., "Massive MIMO communication strategy using polarization diversity for industrial scenarios," *IEEE Antennas and Wireless Propagation Letters*, 14, 2019.
2. Jenssen, R. O. R., et al., "Drone-Mounted Ultrawideband Radar for Retrieval of Snowpack Properties," *IEEE Transactions on Instrumentation and Measurement*, Vol. 69, No. 1, 22130, Jan. 2020.
3. Ghaemi, K., R. Ma, and No. Behdad, "A small-aperture, ultrawideband HF/VHF direction-finding system for unmanned aerial vehicles," *IEEE Trans. on Antennas Propagat.*, Vol. 66, No. 10, 5109–5120, Oct. 2018.
4. Li, W., Y. Hei, P. M. Grubb, X. Shi, and R. T. Chen, "Compact inkjet-printed flexible MIMO antenna for UWB applications," *IEEE Access*, Vol. 6, 5290–5298, Aug. 2018.
5. Saxena, S., B. K. Kanauja, S. Dwari, S. Kumar, and R. Tiwari, "Compact ultra-wideband microstrip antenna with dual polarisation/multi-notch characteristics," *IET Microwave Antennas & Propagation*, Vol. 12, No. 9, 1546–1553, 2018.
6. Shaik, L. A., C. Saha, J. Y. Siddiqui, et al., "Ultra-wideband monopole antenna for multiband and wideband frequency notch and narrowband applications," *IET Microw. Antennas Propag.*, Vol. 10, No. 11, 1204–1211, 2016.
7. Tang, Z., R. Lian, and Y. Yin, "Differential-fed UWB patch antenna with triple band-notched characteristics," *Electron. Lett.*, Vol. 51, No. 22, 1728–1730, 2015.
8. Hung, W.-P., et al., "Non-invasive detection of object by UWB radar," *2017 Asia-Pacific International Symposium on Electromagnetic Compatibility (APEMC), IEEE*, 16971, 2017.
9. Wu, S., et al., "Person-specific heart rate estimation with ultra-wideband radar using convolutional neural networks," *IEEE Access*, Vol. 7, 16848494, 2019.
10. Shehata, M., M. S. Said, and H. Mostafa, "Dual notched band quad-element MIMO antenna with multitone interference suppression for IR-UWB wireless applications," *IEEE Trans. on Antennas Propagat.*, Vol. 66, No. 11, 5737–5746, Nov. 2018.
11. Cai, Y.-Z., H.-C. Yang, and L.-Y. Cai, "Wideband monopole antenna with three band-notched characteristics," *IEEE Antennas Wireless Propag. Lett.*, Vol. 13, 607–610, 2014.
12. Reddy, G. S., A. Kamma, and J. Mukherjee, "Compact printed monopole UWB antenna loaded with non-concentric open-ended rings for triple band-Notch characteristic," *Proceeding in Proc. APMC*, 221–223, Seoul, South Korea, Nov. 2013.
13. Tang, T.-C. and K.-H. Lin, "An ultrawideband MIMO antenna with dual band-notched function," *IEEE Antennas Wirel. Propag. Lett.*, Vol. 13, 1076–1079, 2014.
14. Tripathi, S., A. Mohan, and S. Yadav, "A compact koch fractal UWB MIMO antenna with WLAN band-rejection," *IEEE Antennas Wireless Propag. Lett.*, Vol. 14, 1565–1568, 2015.
15. Terki, A. B., et al., "Design of compact UWB coplanar waveguide-fed modified sierpinski carpet fractal antenna," *2019 IEEE International Symposium on Antennas and Propagation and USNC-URSI Radio Science Meeting, IEEE*, 109192, 2019.

16. Chaturvedi, D., A. Kumar, and S. Raghavan, "An integrated SIW cavity-backed slot antenna-triplexer," *IEEE Antennas Wireless Propag. Lett.*, Vol. 17, No. 8, 1557–1560, Aug. 2018.
17. Kumar, K. and S. Dwari, "Substrate integrated waveguide cavity-backed self-triplexing slot antenna," *IEEE Antennas Wireless Propag. Lett.*, Vol. 16, 3249–3252, 2017.
18. Xuand, F. and K. Wu, "Guided-wave and leakage characteristics of substrate integrated waveguide," *IEEE Trans. Microw. Theory Techn.*, Vol. 53, No. 1, 66–73, Jan. 2005.
19. Wu, J., Y. J. Cheng, and Y. Fan, "A wideband high-gain high- efficiency hybrid integrated plate array antenna for V-band inter-satellite links," *IEEE Trans. Antennas Propag.*, Vol. 63, No. 4, 1225–1233, Apr. 2015.
20. Li, X., J. Xiao, Z. Qi, and H. Zhu, "Broadband and high-gain SIW-fed antenna array for 5G applications," *IEEE Access*, Vol. 6, 56282–56289, Oct. 2018.
21. Chen, Z. and Z. Shen, "A compact cavity-backed endfire slot antenna," *IEEE Antennas Wireless Propag. Lett.*, Vol. 13, 281–284, 2014.
22. Caytan, O., et al., "Half-mode substrate-integrated-waveguide cavity- backed slot antenna on cork substrate," *IEEE Antennas Wireless Propag. Lett.*, Vol. 15, 162–165, 2016.
23. Donelli, M., "A chipless RFID system based on substrate impedance waveguide resonators (SIW)," *IEEE-APS Topical Conference on Antennas and Propagation in Wireless Communications (APWC), IEEE, Proceedings of: IEEE-APS*, 29–32, Verona, Italy, Sept. 11–15, 2017.
24. Sorkherizi, M. S., A. Dadgarpour, and A. A. Kishk, "Planar high-efficiency antenna array using new printed ridge gap waveguide technology," *IEEE Trans. Antennas Propag.*, Vol. 65, No. 7, 3772–3776, Jul. 2017.
25. Bozzi, M., A. Georgiadis, and K. Wu, "Review of substrate integrated waveguide (SIW) circuits and antennas," *IET Microwave Antennas and Propagation*, Vol. 5, No. 8, 909–920, Jun. 2011.
26. Zahirul Alam, A. H. M., et al., "Design of a tuning fork type UWB patch antenna," *International Journal of Electrical, Electronic and Communication Sciences*, Vol. 0, No. 8, 1126–1129, Aug. 2007.
27. Donelli, M. and F. Robol, "Circularly polarized hook antenna for ISM-band systems," *Microwave and Optical Technology Letters*, Vol. 60, No. 6, 1452–1454, 2018.
28. Donelli, M. and J. Iannacci, "Exploitation of RF-MEMS switches for the design of broadband modulated scattering technique wireless sensors," *IEEE Antennas and Wireless Propagation Letters*, Vol. 18, No. 1, 44–48, 2019.
29. Donelli, M., "A broadband modulated scattering technique (MST) probe based on a self complementary antenna," *IEEE-APS Topical Conference on Antennas and Propagation in Wireless Communications (APWC), 2017 IEEE-APS*, 25–28, Verona, Italy, Sept. 11–15, 2017.
30. Donelli, M. and P. and Febvre, "An inexpensive reconfigurable planar array for Wi-Fi applications" *Progress In Electromagnetics Research C*, Vol. 28, 71–81, 2012.
31. Naghar, A., A. Vazquez Alejos, O. Aghzout, and M. Essaaidi, "Compact microstrip omnidirectional ultrawideband antenna with dual broad band nested U-shaped slots and flat frequency response," *Microwave and Optical Technology Letters*, Vol. 57, No. 12, 2854–2856, 2015.
32. Naghar, A., F. Falcone, A. Vazquez Alejos, O. Aghzout, and D. Alvarez Outerelo, "A simple UWB tapered monopole antenna with dual wideband-notched performance by using single SRR-slot and single SRR-shaped conductor-backed plane," *Applied Computational Electromagnetics Society Journal*, Vol. 31, No. 9, 1048–1055, Sept. 2016.
33. Naghar, A., A. V. Alejos, F. Falcone, and O. Aghzout, "Synthesis design of single notched-band UWB antenna using the CSRR dynamic resonance," *10th European Conference on Antennas and Propagation*, Davos, Switzerland, Apr. 11–15, 2016.
34. Naghar, A., A. V. Alejos, F. Falcone, and O. Aghzout, "UWB tapered microstrip antenna with wideband notch using single split ring resonators shaped parasitic conductor," *IEEE APS-URSI*, Fajardo (Puerto Rico), Jun. 26–Jul. 1, 2016.